Remote Sensing of Environment 215 (2018) 330–342

Contents lists available at ScienceDirect

Remote Sensing of Environment

journal homepage: www.elsevier.com/locate/rse

Quantifying understory vegetation density using small-footprint airborne lidar

Michael J. Campbell[a,*], Philip E. Dennison[b], Andrew T. Hudak[c], Lucy M. Parham[b], Bret W. Butler[d]

[a] Department of Geosciences, Fort Lewis College, 1000 Rim Drive, Durango, CO 81301, United States
[b] Department of Geography, University of Utah, 332 South 1400 East, Salt Lake City, UT 84112, United States
[c] Forest Sciences Laboratory, Rocky Mountain Research Station, USDA Forest Service, 1221 South Main Street, Moscow, ID 83843, United States
[d] Missoula Fire Lab, Rocky Mountain Research Station, USDA Forest Service, 5775 Highway 10 West, Missoula, MT, 59808, United States

ARTICLE INFO

Keywords:
Lidar
Discrete return
Small footprint
Understory
Overstory
vegetation density

ABSTRACT

The ability to quantify understory vegetation structure in forested environments on a broad scale has the potential to greatly improve our understanding of wildlife habitats, nutrient cycling, wildland fire behavior, and wildland firefighter safety. Lidar data can be used to model understory vegetation density, but the accuracy of these models is impacted by factors such as the specific lidar metrics used as independent variables, overstory conditions such as density and height, and lidar pulse density. Few previous studies have examined how these factors affect estimation of understory density. In this study we compare two widely-used lidar-derived metrics, overall relative point density (ORD) and normalized relative point density (NRD) in an understory vertical stratum, for their respective abilities to accurately model understory vegetation density. We also use a bootstrapping analysis to examine how lidar pulse density, overstory vegetation density, and canopy height can affect the ability to characterize understory conditions. In doing so, we present a novel application of an automated field photo-based understory cover estimation technique as reference data for comparison to lidar. Our results highlight that NRD is a far superior metric for characterizing understory density than ORD (R^2_{NRD} = 0.44 vs. R^2_{ORD} = 0.14). In addition, we found that pulse density had the strongest positive effect on predictive power, suggesting that as pulse density increases, the ability to accurately characterize understory density using lidar increases. Overstory density and canopy height had nearly identical negative effects on predictive power, suggesting that shorter, sparser canopies improve lidar's ability to analyze the understory. Our study highlights important considerations and limitations for future studies attempting to use lidar to quantify understory vegetation structure.

1. Introduction

Understory vegetation plays a large number of critical roles in forest ecosystems. It is often the most species rich and diverse portion of a forest (Eskelson et al., 2011). Low-lying vegetation cover provides prey species with visual cover to aid in avoiding predation (Lone et al., 2014). For forest-dwelling mammals, much of the nutritious and palatable forage is found in the understory (Nijland et al., 2014). The quantity and size of tree regeneration has important implications not only for forest health, but also economic importance for timber production (Korpela et al., 2012). Understory biomass contributes to carbon sequestration and soil nutrient cycling (Estornell et al., 2011; Suchar and Crookston, 2010). Understory plants also play an important role in maintaining soil structure and reducing erosion (Suchar and Crookston, 2010). Surface fuel loading and bulk density are some of the most important predictors of wildland fire intensity and rate of spread (Keane, 2014). The presence of ladder fuels in the understory of a forested environment can facilitate the transition from a surface fire to a crown fire, which can have dramatic impacts on post-fire ecosystems (Kramer et al., 2016; Stephens, 1998). Understory vegetation density has also been linked to firefighter safety, given that more dense understories can reduce the ability to efficiently traverse wildland environments (Campbell et al., 2017a) and impacts safety zone suitability (Campbell et al., 2017b). For these reasons and many others, it is essential to be able to quantify the abundance and spatial distribution of understory vegetation in forested environments.

As with many biophysical variables, there are two primary approaches for characterizing forest understory vegetation structure: (1) in the field; and (2) through the use of remote sensing technology. Performed in isolation, each approach has its strengths and weaknesses.

* Corresponding author.
E-mail address: mcampbell@fortlewis.edu (M.J. Campbell).

https://doi.org/10.1016/j.rse.2018.06.023
Received 29 December 2017; Received in revised form 11 June 2018; Accepted 17 June 2018

Field-based forest biometry benefits from the accuracy and precision of ground-based, physical mensuration of a targeted set of variables, and being able to control for extraneous, confounding factors. However, field work is both labor-intensive and time-consuming, particularly when considering the limited spatial extent of the data that result from a plot- or transect-based field campaign. The strengths and weaknesses of remote sensing are very much the inverse of those inherent to field work: remote sensing-based analyses of forest structure benefit from broad, "wall-to-wall" spatial coverage, rather than a plot-based sampling of the landscape. However, data collected from a remote perspective does not measure forest biometrics directly; instead, remote sensing data typically characterize objective measures of the interaction of electromagnetic energy with objects on the earth's surface. Indeed, the very nature of a forest understory – existing underneath a forest canopy – complicates the analysis thereof from a remote perspective, where the ability to "see through" the canopy can be severely limited. Accordingly, in order to accurately map understory conditions in complex forested environments, it is necessary to link the objective measures of light interaction provided by remote sensing to field-based measures of specific biometrics, such as vegetation density.

There are many ways to characterize understory vegetation in the field (Higgins et al., 2005). One of the most common methods for doing so is through the use of cover boards, which rely on visually estimating of the relative proportion of a board of known dimensions that is being obscured by vegetation from a given vantage point (Jones, 1968; Nudds, 1977). Cover boards have received widespread use for estimating vegetation density for decades, particularly in the field of wildlife biology, benefitting from their conceptual simplicity and efficiency of field implementation (Duebbert and Lokemoen, 1976; Griffith and Youtie, 1988; Jones, 1968; Musil et al., 1994; Sage et al., 2004; Winnard et al., 2013). Although cover boards have been rarely used as such, they have much potential for use in conjunction with remote sensing technologies such as airborne light detection and ranging (lidar) (Kramer et al., 2016). A widely-acknowledged limitation of cover board analysis, however, is that the subjectivity inherent to the visual estimation of cover board cover is prone to error (Collins and Becker, 2001; Limb et al., 2007; Morrison, 2016). This has motivated the more recent implementation of digital image processing into the semi-automated analysis of cover board photos (Jorgensen et al., 2013).

In recent decades, lidar has emerged as a leading technology in the mapping of three-dimensional vegetation structure. Lidar is particularly useful in characterizing understory structure, as narrow beams of laser light emitted in rapid succession from an airborne sensor can exploit small gaps in a forested canopy. The pulses interact with features in the understory (tree leaves, branches, and boles, shrubs, grasses and forbs) and reflect back to the sensor; the timed pulse returns can provide detailed information on understory structure. Particularly in the past 15 years, as lidar technology and associated data processing capacities have improved, the number of studies involving the use of lidar to characterize understory conditions has grown rapidly (Alexander et al., 2013; Campbell et al., 2017a; Chasmer et al., 2006; Clark et al., 2004; Estornell et al., 2011; Hamraz et al., 2017; Korpela et al., 2012; Kramer et al., 2016; Kükenbrink et al., 2017; Maltamo et al., 2005; Martinuzzi et al., 2009; Morsdorf et al., 2010; Mutlu et al., 2008; Nijland et al., 2014; Riaño et al., 2003; Singh et al., 2015; Su and Bork, 2007). However, like any remote sensing dataset, lidar does not make direct measurements of forest understory structure. Particularly under dense forest canopies, where pulse energy can occlude prior to reaching the understory, it is essential to select appropriate ground reference information capable of linking ground conditions to remotely sensed data. Given their widespread use as an efficient and reliable method for characterizing vegetation density, cover boards could conceivably form an ideal link between ground-based and remotely-sensed measurements. Thus, developing a robust workflow for combining digital cover board analysis to airborne lidar analysis could greatly benefit the many disciplines in which understanding and mapping conditions in the forest understory are critical.

In addition, the selection of relevant lidar-derived metrics for statistical comparison is of critical importance. Many such metrics have been used throughout the literature, but two height stratum-based metrics have dominated in characterizing the understory: overall relative point density (ORD) and normalized relative point density (NRD). A roughly equal number of studies have employed the use of ORD (Hudak et al., 2008; Jakubowksi et al., 2013; Maltamo et al., 2005; Martinuzzi et al., 2009; Mutlu et al., 2008; Riaño et al., 2003; Singh et al., 2015) and NRD (Campbell et al., 2017a; Goodwin et al., 2007; Kramer et al., 2016; Lone et al., 2014; Seielstad and Queen, 2003; Skowronski et al., 2007; Su and Bork, 2007), but none has compared the two for their respective predictive capabilities. Lastly, there are many factors that can affect the accuracy of the resulting understory structural models that must be carefully considered when attempting to characterize the understory, including lidar pulse density, overstory vegetation density, and canopy height. Although these factors are often assumed to affect lidar's ability to model understory conditions, their specific, quantitative effects have only been studied sparingly.

The objectives of this study are to: (1) develop a method for automated cover board photo analysis for use as reference data in lidar understory density estimation; (2) compare two widely-used lidar vertical stratum metrics (ORD and NRD) for their respective abilities to accurately characterize understory vegetation density; and (3) determine the relative effects of lidar pulse density, overstory vegetation density, and canopy height on the ability to accurately characterize understory vegetation density.

2. Background

2.1. Characterizing understory structure using cover boards

There are a number of ways to characterize forest understory structure in the field. Higgins et al. (2005) present a comprehensive review of these methods. Some of the most oft-employed field methods for estimating understory cover are visual obstruction methods. Though the specific methods vary slightly, the assessment is generally based on the determination of the degree to which a distant reference object of known dimensions is being covered by vegetation from a given vantage point. The underlying assumption is that denser vegetation will result in a greater proportion of the object being covered. The two most common reference objects are cover poles (Robel et al., 1970) and cover boards (Jones, 1968; Nudds, 1977), the former enabling obstruction estimation in one dimension, the latter in two. Cover poles are simpler to analyze, given the ease with which one can quantify the proportion of vegetation cover in a single dimension, but cover boards, with their larger sample area, provide more detailed information to the analysis. Cover boards have been used extensively, particularly in wildlife habitat studies (Duebbert and Lokemoen, 1976; Griffith and Youtie, 1988; Jones, 1968; Musil et al., 1994; Sage et al., 2004; Winnard et al., 2013).

The main problem with cover board analyses is the subjectivity of field- or photo-based cover interpretation. Studies have repeatedly demonstrated significant variability in individual analysts' cover estimates Collins and Becker, 2001; Limb et al., 2007; Morrison, 2016. A number of authors have attempted to overcome the issue of interpreter subjectivity by capturing a digital photo of the cover board and subsequently classifying between board and non-board pixels in some semi-automated fashion (Boyd and Svejcar, 2005; Carlyle et al., 2010; Jorgensen et al., 2013; Limb et al., 2007; Marsden et al., 2002; Winnard et al., 2013). Limb et al. (2007) compared this procedure to visual interpretation of a cover board and cover pole, finding that the classification approach greatly reduced the variability in cover estimates and attained the highest degree of correlation with field-sampled biomass. However, many of these studies rely on manually thresholding the pixel value brightness to distinguish between board and vegetation, which can be even more error-prone than visual interpretation (Booth et al.,

2005; Jorgensen et al., 2013). Accordingly, a small number of studies have begun using more advanced image analysis, including supervised classification (Jorgensen et al., 2013).

Another key limitation of cover board-based studies – and, by extension all solely field-based studies – is that they represent a mere sampling of the broader landscape. Remote sensing is one potential solution to this problem, provided that a robust, statistical relationship can be determined between a field-based measure such as cover board cover and some remote sensing dataset capable of characterizing understory vegetation structure, such as lidar. To our knowledge, there has only been one published study to date that has attempted to bridge this divide (Kramer et al., 2016). Kramer et al. (2016) used cover board cover as training data in a lidar-based model aimed at quantifying ladder fuels for fire behavior prediction, demonstrating a high degree of predictive power. In a plot-level study of deer predation, Lone et al. (2014) used both cover board and lidar-derived estimates of understory cover as predictors in a logistic regression model, finding that both variables were strong predictors of predation; however, there was no analysis of the degree to which the two measures were correlated. Given that Kramer et al. (2016) and Lone et al. (2014) employed manual visual interpretation of cover board photos to assess understory cover, no studies, to date, have linked digitally-classified cover board photos to lidar-derived understory metrics.

2.2. Characterizing understory structure using lidar

Airborne discrete-return lidar has been widely used for modeling overstory forest conditions, such as height (Ben-Arie et al., 2009; Hopkinson et al., 2006; Khosravipour et al., 2015; Popescu et al., 2002), basal area (Bright et al., 2013; Chen et al., 2007; Hudak et al., 2006; Lefsky et al., 1999), canopy cover/closure (Ahmed et al., 2015; Holmgren et al., 2003; Korhonen et al., 2011; Smith et al., 2009), species composition (Brandtberg, 2007; Korpela et al., 2010; Vaglio Laurin et al., 2016), and leaf area index (Korhonen et al., 2011; Riaño et al., 2004; Richardson et al., 2009; Tang et al., 2014). However, comparably few studies have examined the ability of lidar to characterize understory conditions. Among these studies, the most common approach to doing so is the area-based approach of Næsset (2002). This method relies on statistically relating one or more lidar-derived metrics within an area of a given size and dimensions to some ground-based vegetation biometric data collected within that same area (Næsset, 2002). The development of an associated predictive model based on that relationship enables broad-scale biometric mapping across unsampled areas (Wulder et al., 2013). A variety of different statistical modeling techniques have been employed to develop these predictive relationships, including more traditional, parametric modeling techniques such as ordinary least squares regression (Clark et al., 2011), multiple regression (Hudak et al., 2006), and stepwise regression (Drake et al., 2002), and more advanced, non-parametric modeling techniques such as *k*-nearest neighbor (Falkowski et al., 2010), support vector machines (Dalponte et al., 2011), and random forests (Martinuzzi et al., 2009). Parametric models have the advantage of conceptual simplicity, being based on statistical relationships between a set of normally-distributed predictor (or independent) variables and a single, normally-distributed response (or dependent) variable, the results of which can be easily interpreted and evaluated for logical consistency (Penner et al., 2013). However, non-parametric models – particularly advanced machine learning algorithms such as random forests – can often result in higher imputation accuracies, albeit at the expense of model transparency and potential for overfitting (Hudak et al., 2008; Latifi et al., 2010).

One of the most important steps in the area-based analytical process is the selection of lidar metrics. Evans et al. (2009) provide an extensive list of metrics that have been used throughout the lidar literature. These metrics, ranging from basic descriptive statistics such as mean, standard deviation, and range, to more advanced parameters such as skewness and kurtosis, can be computed on an entire lidar point cloud extracted within a given *x* by *y* area (e.g. mean lidar point return height within a 30 × 30 m area) (Evans et al., 2009). However, one of the great strengths of lidar is the ability to analyze point clouds in discrete vertical strata. Thus, instead of computing these metrics on the entire vertical extent of a given area, you can first subdivide the point cloud into a series of voxels, based on one or more aboveground height thresholds. This approach is particularly useful when attempting to characterize understory structure in forested environments (Goodwin et al., 2007; Mutlu et al., 2008; Riaño et al., 2003; Seielstad and Queen, 2003; Skowronski et al., 2007).

Two important vertical stratum metrics that are often used in analyzing understory structure are ORD and NRD (USDA Forest Service, 2014). A key assumption of both ORD and NRD is that as vegetation density increases, the likelihood of a given lidar pulse interacting with vegetation increases, thus increasing the proportion of aboveground vegetation point returns. ORD for a given height range between *i* and *j* is defined as the number of points (*n*) that fall between *i* and *j* divided by the total number of points in a given area, from the ground level (height = 0) to the height of the highest point (*k*), as follows:

$$ORD_{(i,j)} = \frac{\sum_i^j n}{\sum_0^k n} \quad (1)$$

NRD is very similar, but it characterizes point density as compared only to the number of points within a given height range and below, defined as follows:

$$NRD_{(i,j)} = \frac{\sum_i^j n}{\sum_0^j n} \quad (2)$$

This is an important distinction, as NRD is theoretically more robust to differences in overstory conditions (USDA Forest Service, 2014). In the presence of a dense overlying canopy, much of the lidar pulse energy is likely to be absorbed in the upper canopy, thus reducing the amount of energy, and in turn the proportion of point returns, in the understory, regardless of actual understory density. Fig. 1 contains a figurative example of lidar point cloud in a conifer forest with both a dense overstory and a dense understory of regeneration. As can be seen, the majority of the point returns are found within the overstory as a result of lidar pulse occlusion. If one were to calculate understory ORD in this example, the result would be relatively low (e.g. 0.1), suggesting that understory density is low, when it is, in fact, relatively high. Conversely, NRD, ignoring the overstory returns, would be much higher (e.g. 0.6), more accurately representing true understory density. Despite the apparent conceptual advantage of NRD over ORD, particularly for characterizing understory structure, there is no clear evidence in the literature as to which metric results in improved model accuracy. Nor is there any sort of agreement on which metric to use, with a similar number of studies using ORD and NRD (see Introduction section for references). No studies to date have directly compared the respective efficacy of ORD and NRD at characterizing understory conditions.

2.2.1. Characterizing understory structure with ORD

Riaño et al. (2003) characterized understory conditions using lidar by first performing a cluster analysis to distinguish between overstory and understory returns, and then computing both understory cover using ORD, and understory height by calculating the 99th percentile of understory returns. Jakubowksi et al. (2013) modeled understory shrub cover and shrub height for fire fuel structural assessment using a modified ORD that calculated point density in a series of different height strata as a proportion of all non-ground points. Maltamo et al. (2005) modeled understory tree number and heights using lidar, finding that ORD bore no significant predictive power for estimating either parameter, instead finding that maximum lidar return height, proportion of all vegetation returns, and height percentiles were more

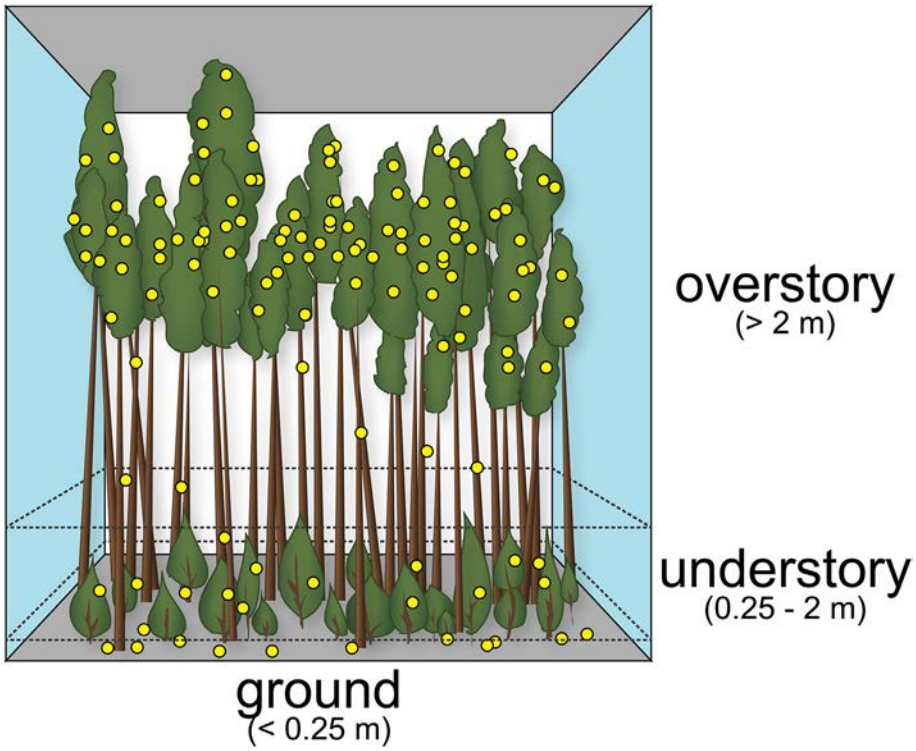

Fig. 1. Three-dimensional lidar point cloud example of a multi-aged lodgepole pine (*Pinus contorta*) forest stand containing both a dense overstory and understory. The yellow circles represent simulated lidar point returns. The dotted lines distinguish between vertical strata representing ground returns (< 0.25 m), understory returns (0.25–2 m), and overstory returns (> 2 m). (For interpretation of the references to color in this figure legend, the reader is referred to the web version of this article.)

effective predictors. Mutlu et al. (2008) fused lidar ORD data calculated in a series of height bins ranging from 0 to 2 m in height with QuickBird imagery to generate a high resolution surface fire behavior fuel type map. Martinuzzi et al. (2009) modeled understory shrub cover and standing dead snags using random forest modeling of a range of predictor variables, determining that three predictors were most valuable for characterizing understory structure: (1) ORD of ground points; (2) ORD between 1 and 2.5 m; and a slope-aspect transformation terrain variable. Singh et al. (2015) included several understory ORD metrics in a random forest model for the detection of an invasive understory plant in North Carolina, but found that they bore little importance in the resultant best-fit prediction model.

2.2.2. Characterizing understory structure with NRD

Seielstad and Queen (2003) provided one of the earliest examples of lidar-based understory vegetation structural characterization, demonstrating how NRD (referred to as "obstacle density") between 0 and 6 ft in aboveground height can be used to distinguish between several of Anderson (1982)'s 13 fire behavior surface fuel models. Goodwin et al. (2007) compared NRD between 0.5 and 4 m in height to field-based ocular estimates of understory cover, finding that NRD alone was a strong predictor of cover. Skowronski et al. (2007) analyzed ladder fuels in the understory through the analysis of a series of vertical strata, finding that NRD between 1 and 2 m in height and NRD between 2 and 3 m in height were strongly correlated to the presence of ladder fuels. Su and Bork (2007) used a clustering technique to separate understory from overstory returns, and further between shrub and herbaceous layers. They attempted to model shrub and herbaceous cover using NRD as the sole predictor; however, no significant relationships were found. Wing et al. (2012) used a modified form of NRD, which involved an intensity-based filter aimed at minimizing the inclusion of ground points.

2.2.3. Effects of pulse density

Airborne lidar is, in essence, a sampling instrument. Laser pulses emitted in rapid succession from an airborne sensor interact with features on or above the ground surface and reflect back to the sensor. The time difference between pulse emission and return, when combined with aircraft GPS location and pulse emission geometry, results in a cloud containing millions of individual points with precise *x*, *y*, and *z* coordinates. The spacing between pulses is a function of emission frequency and angle, as well as aircraft altitude and speed. Lower altitudes and slower speeds result in lower pulse spacing (higher pulse density). With higher pulse density, there are more pulses per unit area to potentially interact with more features on or near the ground, providing a more detailed sampling of the earth's surface. Accordingly, higher pulse density lidar data collections enable the generation of more precise, high-resolution models of three-dimensional structure (Estornell et al., 2011; Hamraz et al., 2017; Kükenbrink et al., 2017; Pesonen et al., 2008; Wing et al., 2012). While this general relationship is widely accepted, the specific effects of pulse density on the ability of lidar to accurately characterize understory structure have scarcely been explored in the scientific literature (Hamraz et al., 2017; Kükenbrink et al., 2017). By comparing airborne lidar to terrestrial lidar in a deciduous forest, Kükenbrink et al. (2017) demonstrated significant effects of airborne lidar pulse density on vegetation volumetric estimation, with low pulse densities (1.3 pulses/m^2) underestimating vegetation volume by 64%, particularly in the understory. Similarly, Hamraz et al. (2017) found that in a dense, mixed conifer-deciduous forest, point densities upwards of 170 points/m^2 would be necessary to accurately identify and segment tree crowns in the understory.

2.2.4. Effects of overstory density

One of the great advantages of using airborne lidar in forested environments is the ability of individual laser pulses to exploit gaps in the overstory to reach understory vegetation and thus facilitate the structural characterization thereof. However, as the density of overstory vegetation increases, the size and number of those gaps decreases. Accordingly, it has been acknowledged by a number of authors that denser canopies reduce the ability to accurately characterize sub-canopy vegetation (Chasmer et al., 2006; Falkowski et al., 2008; Goodwin et al., 2007; Hill and Broughton, 2009; Jakubowksi et al., 2013; Maltamo et al., 2004; Martinuzzi et al., 2009; Mutlu et al., 2008; Richardson and Moskal, 2011; Su and Bork, 2007; Wing et al., 2012).

Chasmer et al. (2006) demonstrated how lidar pulse occlusion in dense forest canopies negatively affects live crown base height estimation. Maltamo et al. (2004) highlighted the degree to which the presence of overstory trees negatively impact both sub-canopy tree identification and height estimation. Falkowski et al. (2008) similarly found that subdominant trees were more difficult to delineate using automated tree identification algorithms as canopy cover increased. Su and Bork (2007) compared lidar-understory cover model predictive power between open- and closed-canopy aspen forests; however, they were unable to obtain any statistically-significant predictive relationships in either environment, thus nullifying the comparative ability. Korpela et al. (2012) provide a detailed analysis of lidar pulse transmission in a forested environment, highlighting the effects of species-specific canopy cover on the likelihood of given pulses interacting with features in the understory. They also suggest a potentially significant effect of scan angle, indicating that including a variety of scan angles may provide more opportunity for canopy penetration. Wing et al. (2012) found no effect of canopy cover on understory cover prediction accuracy; however, they suggest that this may be a unique effect of the distinct vertical stratum differences between understory and overstory vegetation in the ponderosa pine (*Pinus ponderosa*) forests they were studying.

Several studies have quantified the effect of overstory vegetation cover and/or density on the resultant accuracy of lidar-derived digital terrain models (DTMs) (Clark et al., 2004; Hopkinson et al., 2006; Reutebuch et al., 2003; Su and Bork, 2006; Takahashi et al., 2006). These studies consistently demonstrate decreasing DTM accuracy with increasing overstory cover. However, very few studies have explicitly tested the effect of overstory conditions on the ability to characterize the understory, with the exception of Su and Bork (2007) who found no effect and Wing et al. (2012) who suggest that the specific vegetation type they studied may be anomalous with respect to its overstory-understory relationship. One of the key challenges of examining the effect of overstory density on the ability of lidar to characterize understory density is that there tends to be a negative correlation between overstory density and understory density, because as canopy cover increases, less light is able to reach the forest floor, limiting the ability of light-dependent understory plants to regenerate (Alexander et al., 2013; Bartemucci et al., 2006; Kerns and Ohmann, 2004; Martinuzzi et al., 2009; Wing et al., 2012). Accordingly, when analyzing the effects of overstory lidar occlusion, one must be aware of this potentially confounding ecological relationship.

2.2.5. Effects of canopy height

While much of the canopy occlusion effect can be explained by overstory density, we hypothesize that there is an additional, independent effect of canopy height. This effect is likely to manifest primarily on off-nadir (higher emission angle) pulses. In the presence of very tall trees, even if those trees are widely spaced (low density), an angular lidar pulse is more likely to interact with multiple overstory surfaces prior to reaching the understory (Fig. 2). For example, in a forest of 150 ft tall trees, a 20° pulse can interact with two trees almost 55 m apart. This may be a partial explanation for the lack of an effect of overstory cover on the ability to accurately characterize understory conditions found by Wing et al. (2012). They were working in forests typically characterized by tall and widely-spaced ponderosa pine trees. Although many have implicated the effects of overstory vegetation on lidar-based understory characterization, none have explicitly related the effect to a continuous measure of canopy height.

3. Methods

3.1. Study area

This study was conducted in the Monroe Mountain area of Fishlake National Forest in central Utah (Fig. 3). This area was selected primarily due to the availability of recent, high quality lidar data collected during leaf-on conditions. The lidar data were acquired by Digital Mapping, Inc. on behalf of the USDA Forest Service and Utah Automated Geographic Reference Center between August and September of 2016 with an average point density of 16.43 pts/m^2. The 711 km^2 area ranges in elevation from 1711 m to 3418 m. The dominant vegetation types within the study area include black sagebrush (*Artemisia nova*) and big sagebrush (*Artemisia tridentata*) shrublands, pinyon-juniper (*Pinus edulis* and *Juniperus osteosperma*), Gambel oak (*Quercus gambelii*), and curlleaf mountain mahogany (*Cercocarpus ledifolius*) woodlands, and quaking aspen (*Populus tremuloides*), Engelmann spruce (*Picea engelmannii*), white fir (*Abies concolor*), and subalpine fir (*Abies lasiocarpa*) forests. The area has seen significant changes in vegetation conditions over the past few decades, including widespread beetle-induced Engelmann spruce mortality, and aspen decline due to decreased fire frequency and increased grazing (USDA Forest Service, 2017). In recent years, along with a number of partner organizations, the Forest Service has enacted extensive forest management in the Monroe Mountain area, including mechanical treatment and prescribed burning, to promote aspen regeneration. These changes have combined to produce a landscape mosaic of diverse forest types and conditions in both the understory and overstory.

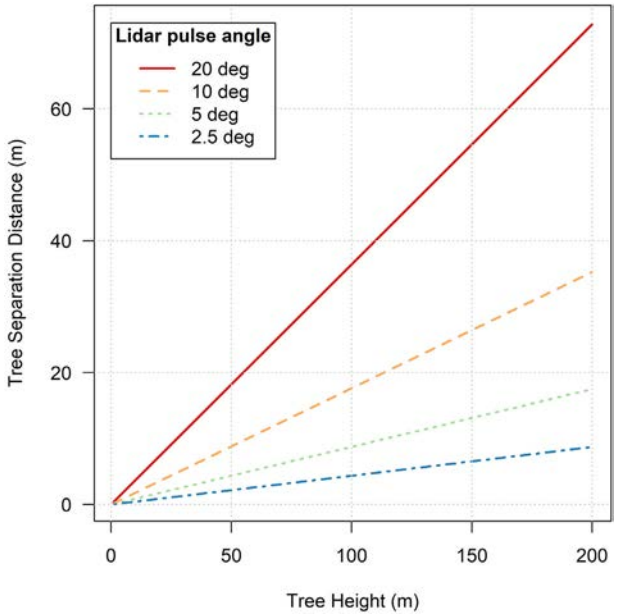

Fig. 2. The relationship between tree height and theoretical tree separation distance under which individual lidar pulses could interact with multiple trees at various scan angles.

3.2. Field data

3.2.1. Field site selection

In order to facilitate direct comparison to the lidar data, field data were collected exactly one year after the lidar data were acquired (between August and September of 2017). Field sites had to meet the following criteria to facilitate accessibility, promote data collection efficiency, and reduce potential edge effects. Sites had to be: (1) within 100 m of major roads; (2) at least 25 m from all roads and water features; (3) on slopes of < 10°; and (4) on public lands. By imposing these site selection criteria, it is possible that vegetation structure sampled in our study is not representative of the study area as a whole, including areas that exceeded the sampling constraints (e.g. steeper slopes). In addition, with the primary goal being to analyze understory vegetation in forested environments, sites had to be located within areas where vegetation equal to or > 2 m in height occupied at least 20% of a given

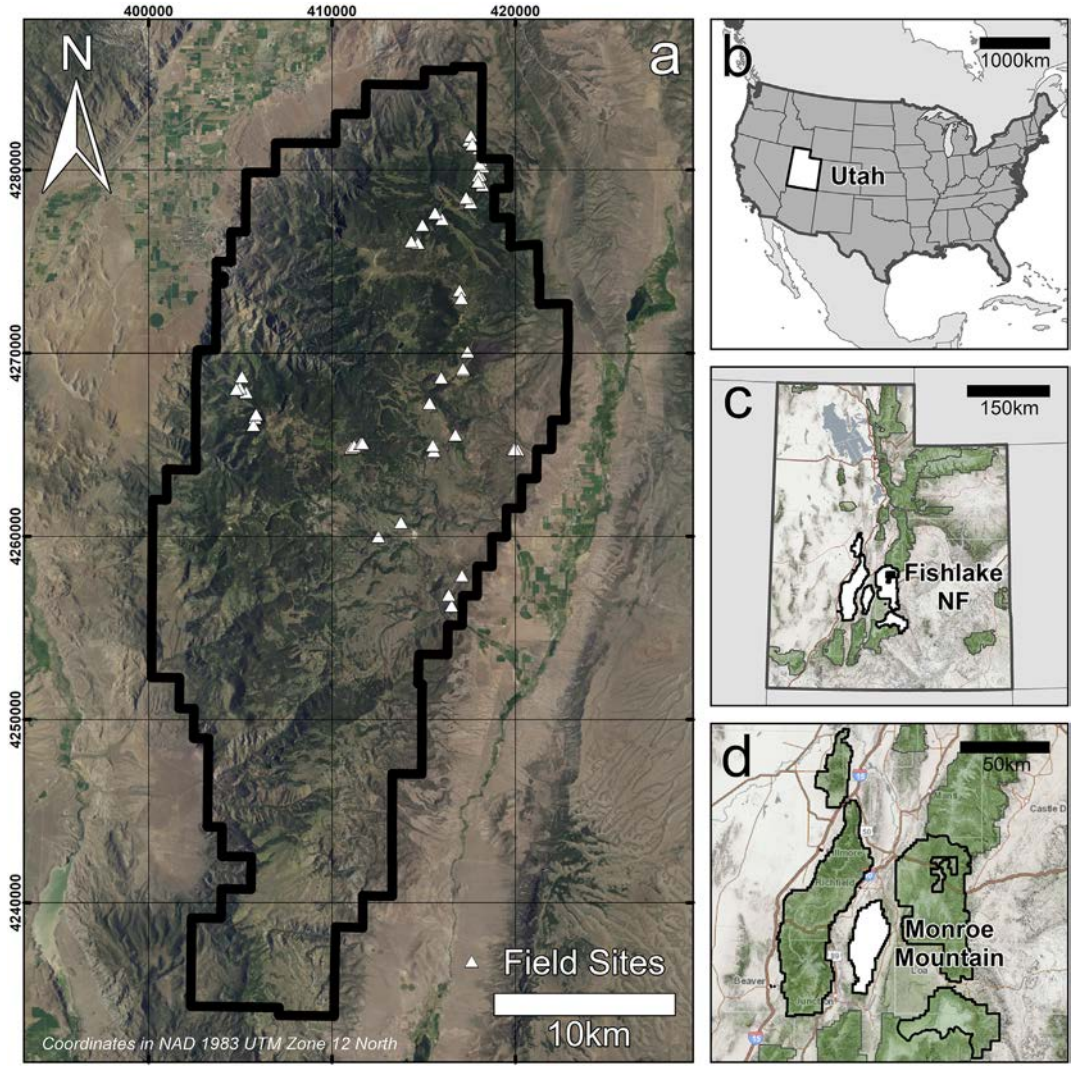

Fig. 3. Study area map of the Monroe Mountain area (a) within Fishlake National Forest (d), in the state of Utah (c), United States (d).

30 × 30 m area. This required the creation of a canopy height model (CHM) from lidar. A study area-wide CHM was generated at a 1 m spatial resolution as the difference between a DTM, interpolated from lidar points classified as "ground" points, and a digital surface model (DSM), interpolated from all first-return lidar points. In this remote, largely undeveloped study area, we assumed that first-return points are either vegetation or bare ground. As such, no filtering of first-return points by surface type (e.g. "vegetation" vs. "building") was performed prior to interpolating a DSM, given the lack of manmade structures in the area. A height-based classification was performed to classify CHM pixels as either tree (≥ 2 m) or non-tree (< 2 m). A percent tree cover map was then generated by calculating the relative proportion of 1 m tree pixels within each 30 × 30 m cell of an aggregated raster grid throughout the study area.

Within the resulting area of eligibility for field site placement, we employed a conditioned Latin hypercube sampling (CLHS) strategy in order to capture a broad range of vegetation conditions. CLHS is a stratified random sampling procedure that enables the selection of samples that simultaneously maximize the variability captured in each of a defined set of variables (Minasny and McBratney, 2006). All of the following CLHS input datasets were generated at a spatial resolution of 30 m, in order to identify patches of forest within which to place transects that maximized topographic and vegetation diversity: (1) lidar-derived elevation; (2) lidar-derived understory (0.15–1.85 m) NRD (NRD_{under}); (3) lidar-derived overstory (> 1.85 m) NRD (NRD_{over}); (4) lidar-derived vegetation height; and (5) Landsat 8 OLI-derived normalized difference vegetation index (NDVI). NDVI was added to ensure that not only would a variety of vegetation structural settings be sampled, but also different vegetation types. For example, conifer and aspen forests may appear structurally similar using lidar alone, but typically possess significantly different NDVI values due to their unique reflectance properties. All lidar data processing was performed using *LAStools* (Isenburg, 2015).

Fifty sample point locations were identified within the area of eligibility using the CLHS algorithm, strategically placed to maximize the variability captured among the five aforementioned vegetation variables, as implemented in the *clhs* package in R statistical software (R Core Team, 2016; Roudier, 2017) (Fig. 3). Each point was then converted to a 10 m transect line, by extending a line 5 m in each direction perpendicular to the terrain aspect (along the contour), to ensure relatively flat transects. Aspect was calculated from the lidar-derived DTM.

3.2.2. Cover board photos

Cover boards are most often designed to facilitate visual photo interpretation, typically comprising a grid of alternately-colored boxes, like a checkerboard. Thus, when analyzing a cover board photo, one can readily judge how many boxes, or what portions of each box, are covered by vegetation, the averaging of which can provide an estimate of overall cover for the entire board. However, in order to reduce the

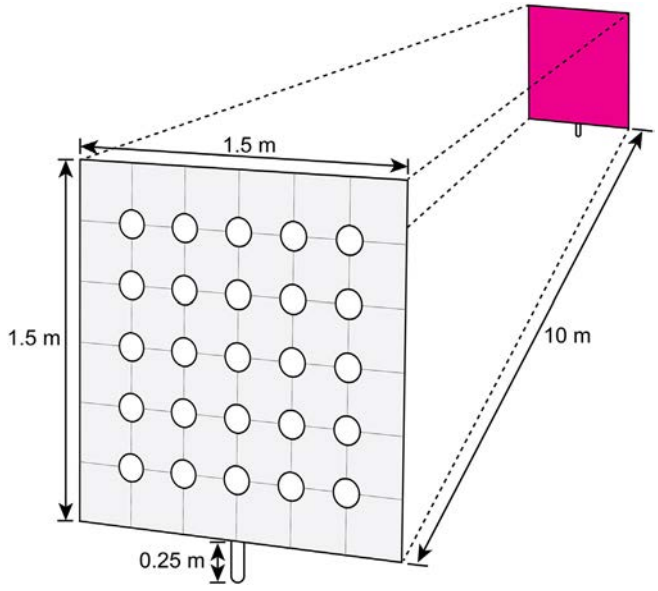

Fig. 4. Cover board photo setup.

potential for interpretation error and/or observer bias in cover estimation, we opted to create a cover board that could be analyzed in an objective, automated fashion. To do so, the board needed to be both easily distinguished from natural vegetation, and a single, uniform color. Through preliminary experimentation with several different cover board colors (neon yellow, orange, blue, and magenta) it was determined that a magenta-colored cover board would be the most spectrally separable from vegetation. This experiment was performed using the approach described in this section (3.2.2) and the next (3.2.3), after which an accuracy assessment of the resulting classified cover board photos revealed that the magenta board yielded the highest classification accuracy. Accordingly, we created a 1.5 × 1.5 m magenta cover board using heavy-duty canvas and PVC pipes (Fig. 4). In addition, our preliminary work highlighted the fact that small differences in viewing angle could result in significant differences in the resultant cover estimate. Accordingly, we created a 1.5 × 1.5 m photo viewing grid, also using canvas and PVC, with 25 equally-spaced, round, 10 cm-diameter viewing holes through which cover board photos would be taken (Fig. 4).

We navigated to each transect start point, staked the photo viewing grid into the ground, ensuring that the stake was perfectly vertical using a bubble level, and collected a GPS point using a Trimble Geo7x with 200+ point averaging. We then used a tape to measure 10 m from the start point to the end point using a compass to navigate in the direction of the azimuth defined during the transect generation process. We then staked the cover board into the ground and collected another GPS point. Lastly, we took photos through each of the viewing grid holes towards the cover board, totaling 25 photos per site using a SONY HX-50V digital camera, with a fixed, 8× optical zoom. In order to ensure that each photo had the same lens-cover board distance (10 m), the camera was placed such that the lens was in line with the vertical plane of the photo grid, centered in the viewing hole.

3.2.3. Photo classification

As a result of the field data collection effort, there were 1250 cover board photos (50 sites × 25 photos). Rather than attempt to visually estimate the cover in each of these photos, an automated "board" vs. "non-board" classification was performed as follows. A program was written in R using the *raster* package (Hijmans et al., 2016) to load each photo sequentially, and generate 4 random points within a square area generally occupied by the cover board (square length and height equal to 2/3 of the photo height). Each point was then visually interpreted as either "board" or "non-board". "Non-board" is an inclusive class that represents pixels containing anything besides the cover board, primarily live and dead vegetation. There were 5000 photo interpreted points in total, 4800 of which were randomly designated as training data, and 200 of which were designated as accuracy assessment data (100 "board" points, 100 "non-board" points).

Table 1
Spectral variables used in stepwise logistic regression to classify board vs. non-board on cover board photos.

Variable	Abbreviation	Calculation
Red	R	8-bit R pixel mean
Green	G	8-bit G pixel mean
Blue	B	8-bit B pixel mean
Normalized red	R_{norm}	R / (R + G + B)
Normalized green	G_{norm}	G / (R + G + B)
Normalized blue	B_{norm}	B / (R + G + B)
Magenta	M	(R + B) / 2
Cyan	C	(B + G) / 2
Yellow	Y	(G + R) / 2
Normalized magenta	M_{norm}	M / (M + C + Y)
Normalized cyan	C_{norm}	C / (M + C + Y)
Normalized yellow	Y_{norm}	Y / (M + C + Y)
Normalized difference red-green	NDRG	(R – G) / (R + G)
Normalized difference green-blue	NDGB	(G – B) / (G + B)
Normalized difference blue-red	NDBR	(B – R) / (B + R)
Normalized difference magenta-cyan	NDMC	(M – C) / (M + C)
Normalized difference cyan-yellow	NDCY	(C – Y) / (C + Y)
Normalized difference yellow-magenta	NDYM	(Y – M) / (Y + M)

For each of the 4800 training points, red, green, and blue (RGB) pixel value means were extracted within a 5 × 5 pixel square immediately surrounding it. A number of derivative variables were also calculated to improve classification accuracy (Table 1). We performed a stepwise logistic regression, beginning with a full model that contained all of the independent variables in Table 1 and iteratively removing them until an optimal balance between model complexity and variance explained, as approximated by the Akaike Information Criterion (AIC). The resulting model was used to classify "board" and "non-board" for every pixel in all 1250 photos. We assessed overall and class-specific user's and producer's accuracies of the photo classification using the accuracy assessment data.

Given that every photo was taken from a fixed distance (10 m), with a consistent zoom (8×), towards a board of the same size (1.5 × 1.5 m), relative cover could be easily calculated, provided that a relative scale could be determined between photo pixel size and cover board size. To calculate this scale, we first needed to identify a single photo from each transect that had at least one entire cover board dimension (either a full width or height) visible. There were only 4 transects where no such dimensions were clearly visible. For the remaining 46, a measurement was taken in Adobe Photoshop of equivalent number of pixels for each cover board height or width, depending on which was more clearly visible. From this, an effective per-pixel area could be calculated. This effective pixel area was then multiplied by the number of pixels classified as "board" for each photo, which was then compared to the entire board area (2.25 m^2) to determine relative cover. Overall understory cover was then calculated for each transect by taking the mean value for all 25 photos.

3.3. GIS and lidar data processing

The GPS points representing transect start and end points were differentially corrected to a mean absolute positional error of 52 cm using base station data from nearby Scipio, UT and converted to shapefile format for use in GIS. A line was drawn between points representing the transect, and a buffer created around each transect within which the lidar data would be analyzed. A 0.75 m rectangular buffer was generated around the transect line to represent the precise

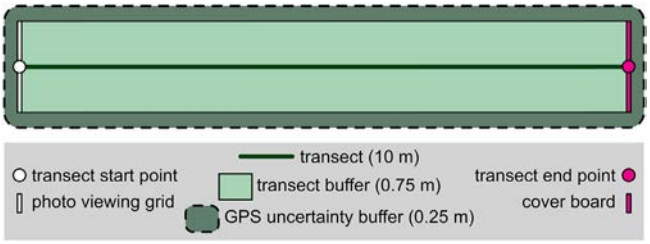

Fig. 5. Transect layout.

area between cover board and photo grid (10 m long × 1.5 m wide). However, given the small uncertainty in the GPS data, we performed an additional buffer around the rectangle of 0.25 m (Fig. 5).

Lidar point cloud data were extracted within each transect plus GPS uncertainty buffer. The following metrics were derived for each transect point cloud: (1) understory NRD from 0.15–1.85 m (NRD_{under}); (2) understory ORD from 0.15–1.85 m (ORD_{under}); (3) overstory ORD from > 1.85 m (ORD_{over}); (4) 95th height percentile; and (5) pulse density. Even though the cover board ranged in height from 0.25–1.75 m, we opted to add 10 cm to both ends to account for small uncertainty in the vertical accuracy of lidar returns and to create a more inclusive voxel to increase the number of point returns analyzed. We did not calculate overstory NRD because overstory ORD and NRD are the same metric, since it was inclusive of all points higher than 1.85 m.

3.4. Analysis

In order to assess their respective abilities to predict understory vegetation density, individual ordinary least squares regression models were generated for ORD_{under} and NRD_{under}. Both ORD and NRD displayed non-normal, right-skewed distributions. Accordingly, log regression was performed in both cases. The models were compared according to the degree to which the lidar-based independent variables were able to explain variance in the cover board-based dependent variable, as approximated by R^2, and AIC.

In order to determine the relative effects of lidar pulse density, overstory vegetation density, and canopy height, we performed a bootstrapping analysis. This approach allowed us to assess the effects of these limiting factors on the ability to accurately model understory vegetation density using lidar by successively generating random subsets of data, each of which possessed a slightly different set of lidar and vegetation conditions, and each of which yielded a slightly different statistical relationship between understory NRD and cover board density. Ten-thousand random samples of 20 were taken, without replacement, from the 50 original transect-level data points. For each sample data subset, the mean pulse density, the mean overstory ORD, and the mean 95th height percentile were calculated. In addition, a regression model was generated comparing understory NRD (independent variable) to cover board cover (dependent variable) for each subset as well, from with R^2 values were computed. We then compared the subset data pulse density, overstory ORD and 95th height percentile to the resultant model R^2 in a series of individual ordinary least squares regression analyses to determine the relative effects of these variables on the degree to which understory NRD can predict understory vegetation density in a series of regression analyses. Lastly, in order to account for the potentially confounding effects arising from correlation between overstory ORD and 95th height percentile, we performed a multiple regression containing all three predictor variables (pulse density, overstory ORD, and 95th height percentile).

4. Results

In total, 1250 photos were classified according to a binary “board” vs. “non-board” classification (Fig. 6). Of the 18 spectral variables generated for each photo, a stepwise regression algorithm determined that a combination of 8 variables was best for distinguishing between those image pixels that contained primarily board and those that contained primarily non-board (predominantly vegetation) (Table 2). Each predictor variable was significant at a level of $\alpha = 0.1$. The model coefficients were used to develop a prediction equation, as follows:

$$y = 0.039R - 0.077G + 0.052B + 423.9R_{norm} + 8.678NDGB + 57.57NDBR - 237.0NDMC - 62.63NDYM - 0.015 \quad (3)$$

where variable names are listed in Table 2. Resulting pixel values greater than or equal to 0.5 were classified as board (1); those pixels with values < 0.5 were classified as non-board (0). Randomly-selected accuracy assessment points were compared to the resultant classification (Table 3). Overall accuracy was high, at 97.5%. Inaccuracies arose solely in the over-mapping of pixels classified as non-board, suggesting that the resulting classified images tended to slightly overestimate cover by a small margin.

For each transect, a single density estimate was obtained by taking the mean percent cover for each of the 25 gridded photos. Transect-level cover board density was then compared to lidar-derived ORD_{under} and NRD_{under} (Fig. 7). NRD_{under} far outweighed ORD_{under} in terms of predictive power (R^2: 0.442 vs. 0.137) and model quality (AIC: −15.802 vs. 5.966). ORD_{under} bore almost no recognizable relationship to cover board density (Fig. 7a).

The results of the bootstrapping analysis to determine the relative effects of pulse density, overstory vegetation density, and canopy height on the ability to accurately model understory density can be seen in Fig. 8 and Table 4. Although there is much spread in the resulting scatterplots, each variable was found to have a statistically significant relationship to the NRD-cover board density model R^2 values in a multiple regression environment ($\alpha = 0.001$). As the standardized coefficients suggest, pulse density had the effect of greatest magnitude on R^2, followed by overstory density and canopy height, which had very similar effects. Accordingly, as pulse density increases, the ability to model understory density using lidar NRD_{under} increases. Conversely, as overstory vegetation density (as approximated by lidar ORD_{over}) increases, the ability to model understory density using lidar NRD_{under} decreases. And lastly, as canopy height (as approximated by lidar 95th height percentile) increases, the ability to model understory density using lidar NRD_{under} decreases.

5. Discussion

Lidar is unique in its ability to characterize understory structure at a high spatial resolution across broad tracts of forest land. While this ability has widespread application in fields ranging from wildlife biology to wildland firefighter safety, there are some key considerations that require addressing before engaging in such an analysis. We have presented and quantified the effects of a number of these considerations in this study. The first consideration is the selection of appropriate understory lidar metrics for use in modeling understory vegetation density. We compared two widely-used metrics, ORD to NRD, for their respective abilities in predicting understory density as measured in the field, finding that NRD was far superior in this regard. NRD was able to explain nearly half of the variance in field-measured understory density, whereas ORD explained next to none. This significant difference is likely a result of overstory conditions. Many authors have pointed to the fact that overstory vegetation can result in lidar pulse energy occlusion, thus limiting the ability to characterize understory conditions (e.g. Hamraz et al., 2017; Kükenbrink et al., 2017). NRD accounts for differences in overstory vegetation, as it only takes into consideration those portions of a given lidar pulse that have already penetrated the canopy in computing relative proportion. ORD does not. Accordingly, if one's goal is to characterize understory conditions in a forested environment – particularly one with a dense overstory – the results of our

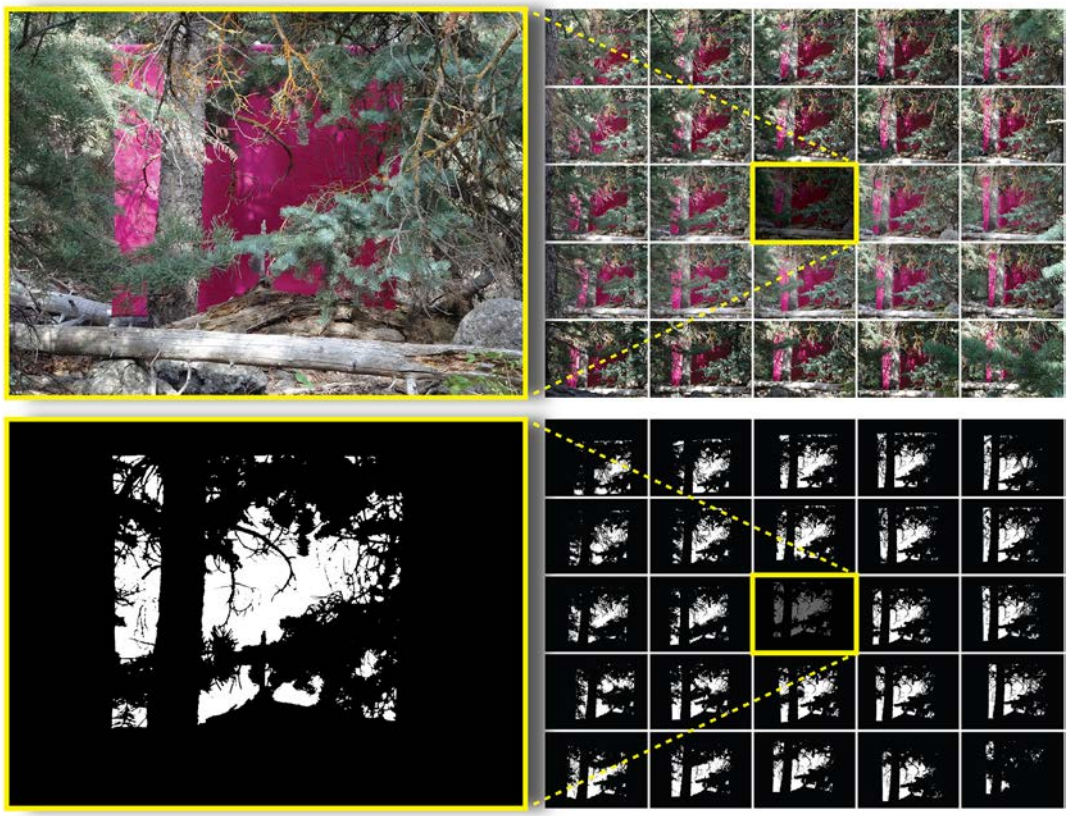

Fig. 6. Cover board photo classification example results. In the lower two panels, white indicates pixels classified as "board" and black indicates pixels classified as "non-board".

Table 2
Stepwise logistic regression model results for cover board photo classification. Null deviance = 6131.12 on 4799 degrees of freedom. Residual deviance = 658.92 on 4791 degrees of freedom.

Model parameter	Coefficient	Standard error	z Value	p
Intercept	−0.015	38.00	−3.907	< 0.001
R	0.039	0.009	4.456	< 0.001
G	−0.077	0.015	−5.127	< 0.001
B	0.052	0.016	3.323	< 0.001
R_{norm}	423.9	113.6	3.730	< 0.001
NDGB	8.678	4.980	1.743	0.081
NDBR	57.57	24.56	2.344	0.019
NDMC	−237.0	58.06	−4.082	< 0.001
NDYM	−62.63	16.24	−3.856	< 0.001

Table 3
Cover board photo classification accuracy assessment.

		Reference data		Accuracy		
		Board	Non-board	User	Producer	Overall
Classified data	Board	95	0	100.0%	95.0%	97.5%
	Non-board	5	100	95.2%	100.0%	

study suggest using NRD. In the absence of an overstory, however, NRD and ORD are, in fact, the exact same measure.

The results of our study also suggest that NRD, though preferable to ORD, does not account for all overstory effects. The very fact that NRD only accounted for roughly half of the variance in field-measured density highlights this fact. This relatively low R^2 is not uncommon among lidar-based studies of understory vegetation and highlights the complexity of undertaking such an endeavor. In order to determine what factors contributed to this limited explanatory power, we examined the effects of two overstory conditions on understory model fit. Using a bootstrapping analysis, we found that as overstory density and canopy height increase, the ability to effectively model understory conditions decreases. In addition, as pulse density increases, so too does the ability to model understory conditions. Thus, it comes as no surprise that superior the ability of NRD to accurately quantify understory density is maximized with a high pulse density lidar dataset in areas with shorter, sparser canopies. For example, if we take the uppermost 97.5 percentile of pulse density (17.90 pulses/m^2) and the lowermost 2.5 percentile of overstory density (0.38) and canopy height (9.04 m) in our bootstrapped data – representing "ideal" conditions while avoiding extrapolation – the resultant R^2 for using NRD to predict understory would be 0.59, according to our multiple regression results. Presumably, with an even higher pulse density, and even lower overstory density and canopy height, this relationship could improve even more.

However, even in these optimal conditions, a noteworthy amount of variance is still left unexplained. There are several reasons why this may be the case. First, as in all lidar-based studies but particularly in those that examine near-ground vegetation conditions, the accuracy of the classification between ground and non-ground points is critical (Meng et al., 2010). The ground point classification is the basis upon which lidar point aboveground heights are calculated prior to calculation of metrics for predictive modeling. Particularly when working in as narrow of a height range with a low-end threshold as low as we did in this study (0.15–1.85 m), a few misclassified ground points can have a dramatic effect on resultant NRD calculations. The dataset we used in this study has a self-reported vertical root mean square error of 6.1 cm for ground points, and a 95% confidence interval of ± 11.9 cm. Thus, it is highly likely that some of the points we considered aboveground vegetation were in fact ground points, and vice versa. In this study area

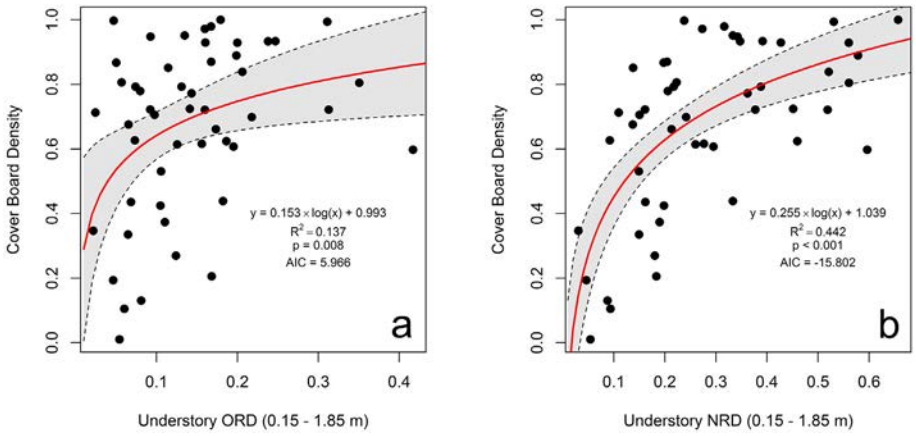

Fig. 7. Comparison between ordinary least squares regression models predicting cover board density using lidar-based understory overall relative point density (ORD) (a) and normalized relative point density (NRD) (b).

in particular, there was an abundance of downed coarse woody debris, which a ground filtering algorithm may have difficulty distinguishing from the ground (Pesonen et al., 2008).

A second factor than may have negatively impacted the lidar-understory density relationship found in our study stems from the nature of our field data. As discussed earlier, cover boards are an invaluable tool for characterizing understory conditions, widely used for their efficiency of implementation, conceptual simplicity, and applicability in a range of disciplines. Our study represents one of the first attempts at using cover boards as ground reference data for direct comparison to lidar, with Kramer et al. (2016) being the only other published example to date. While it shows great promise as a source of training and validation data, there are limitations that emerge, primarily from the effects of viewing geometry. To avoid biasing our dataset towards open understories, we made every attempt to place our viewing grid on the precise, computer-generated GPS location to the extent that it was physically possible. Likewise, we attempted to place the cover board exactly 10 m from the viewing grid along a pre-defied azimuth. While this facilitated an unbiased sample, occasionally it resulted in, for example, the viewing grid falling right behind the bole of a tree. Thus, even in a relatively open stand, cover could appear relatively high, due to the relationship between viewing geometry and tree proximity. Fig. 9 demonstrates one such example, where mean cover is increased almost entirely due to the presence of a single tree bole. Our use of a 25-photo, multi-angle viewing grid was explicitly aimed at reducing these effects. And, in fact, the calculation of standard deviation between individual photo cover estimates allowed us to quantify the effects of this viewing geometry-based structural complexity on lidar-understory density model fit. As can be seen in Fig. 10, as structural complexity increases, the ability to accurately characterize understory density using lidar decreases.

Table 4
Results of multiple regression analysis between bootstrapped R^2 values and pulse density, overstory density, and canopy height ($R^2 = 0.104$, $p < 0.001$).

Model parameter	Coefficient	Standardized coefficient	Standard error	t Value	p
Intercept	0.029	0.476	0.054	0.525	0.6
Pulse density	0.050	0.024	0.003	17.64	< 0.001
Overstory density	−0.489	−0.018	0.048	−10.15	< 0.001
Canopy height	−0.017	−0.017	0.002	−9.281	< 0.001

A third potential factor that may have contributed to the disagreement between lidar and cover board density estimates is the difference in vegetation conditions between when the field and remote sensing data were collected. Although we attempted to minimize the differences between vegetation phenological conditions between these two time frames by collecting the field data exactly one year after lidar data collection, conditions could have been slightly different during August–September in 2016 and 2017. In fact, an analysis of MODIS Terra enhanced vegetation index (EVI) 16-day average data (MOD13Q1 product) captured within the Monroe Mountain area (as defined by the study area boundary, Fig. 3) between 2016 and 2017 revealed that average EVI values were slightly higher in August–September of 2017 ($EVI_{2017} = 0.235$) than August–September of 2016 ($EVI_{2016} = 0.219$) (ORNL DAAC, 2017). EVI is a good predictor of leaf area index (Zhang et al., 2003), which suggests that leaf index may have been higher during field data collection than during the lidar data collection.

Although every attempt was made to maximize the variety of

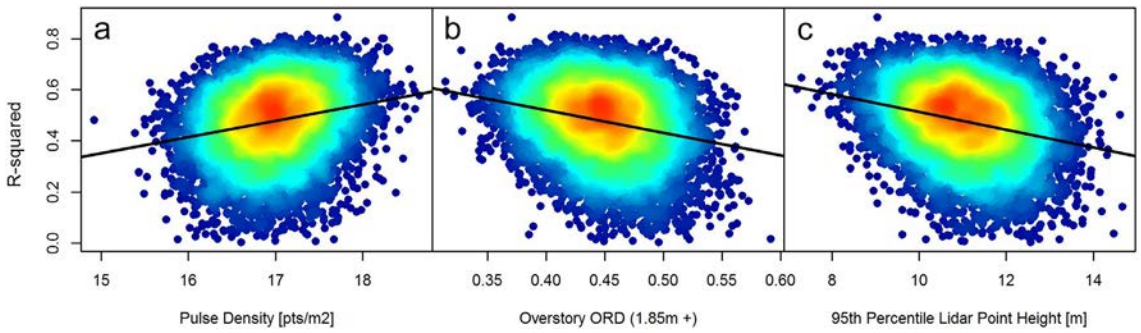

Fig. 8. The bootstrapped effect of lidar pulse density (a), overstory canopy density (as approximated by lidar overall relative point density of all points higher than 1.85 m) (b), and canopy height (as approximated by 95th percentile of lidar point return height) (c) on the ability of lidar to model understory cover (as approximated by the amount of variance in cover board cover explained by lidar understory normalized relative point density).

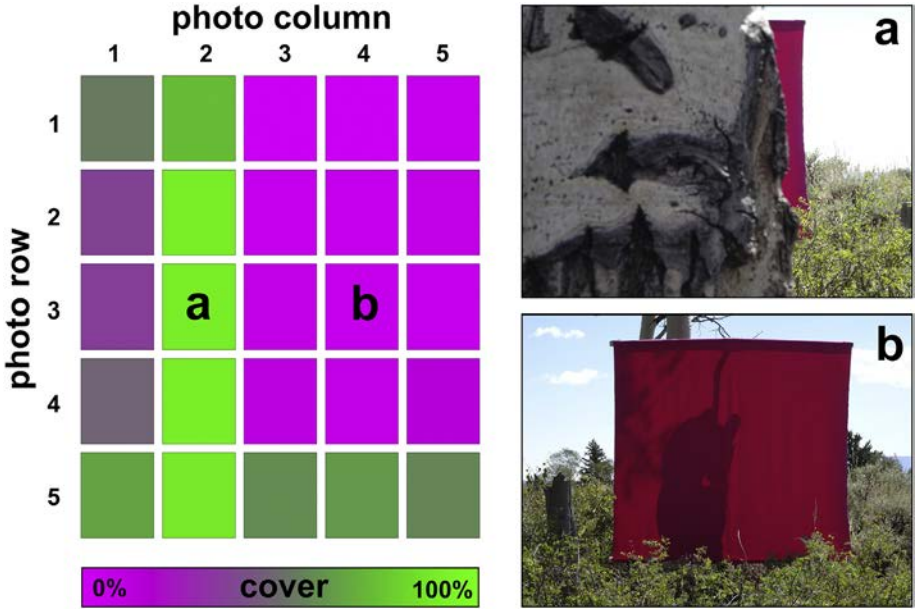

Fig. 9. Photo-by-photo cover estimates for an example transect (Transect #37) that demonstrate the effect that a single tree can have on overall, transect-level cover estimates, with two example photos highlighting high (a) and low (b) cover within the same transect.

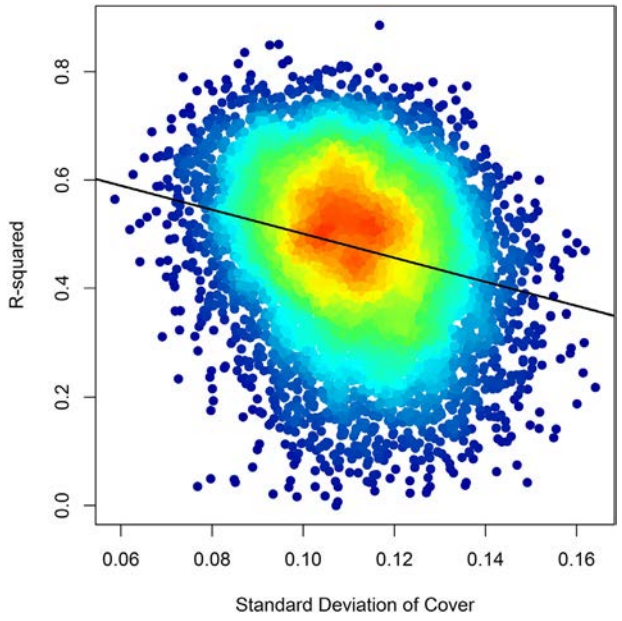

Fig. 10. The effect of understory complexity, as approximated by the standard deviation of cover derived from individual photo cover estimates, on the ability to characterize understory density using lidar NRD.

conditions sampled in our study, continued study is needed in a broader range of vegetation conditions – especially overstory conditions – to expand the spatial applicability of the results we obtained from our study area in Monroe Mountain, UT. For example, the highest overstory lidar ORD found in our study area was 0.80, which is to say that the densest canopy we encountered still allowed 20% of point returns to penetrate through to the understory and ground. In a dense, broadleaf, tropical environment, for example, one might expect that there would be some canopies so dense that no lidar energy at all could penetrate them. However, no such density was found in the Rocky Mountain mixed conifer-aspen forests found in our study area. That being said, the objective, quantitative nature of the lidar and cover board-based measures of vegetation density presented in this study are thought to be fairly vegetation condition- and type-independent, making the workflow presented in this research a viable option in a wide range of environments. In addition, while the use of cover boards as ground reference data for lidar-based quantification of understory vegetation density is promising, more research is required to determine methodological optimality (e.g. plot layout, board material/color/dimensions).

6. Conclusions

Lidar is an incredibly powerful remote sensing dataset capable of assessing a wide range of vegetation structural conditions; however, it is not without its limitations. In this study, we inquired into several important considerations that studies aimed at quantifying understory structure in forested environments must take into account. Specifically, we highlight that lidar NRD is far superior to ORD in terms of its modeling capacity. This is a particularly impactful result, as no one has yet quantitatively compared the two, and yet each is widely used throughout the lidar literature. We also provide robust, quantitative backing to the oft-cited but scarcely-quantified effects of pulse density, overstory vegetation density, and canopy height on the ability to characterize forest understory vegetation density.

Acknowledgments

Funding for this research was provided by the US Forest Service National Fire Plan through the Office of Research, the National Wildfire Coordinating Group Fire Behavior Subcommittee, and the Wildland Fire Management Research Development & Application Program, Cooperative Agreements 14JV11221637123 and 15CR11221637105. The funding sources had no direct involvement in the study design, data collection, analysis or interpretation, manuscript writing, or decision to submit the article for publication.

References

Ahmed, O.S., Franklin, S.E., Wulder, M.A., White, J.C., 2015. Characterizing stand-level forest canopy cover and height using Landsat time series, samples of airborne LiDAR, and the Random Forest algorithm. ISPRS J. Photogramm. Remote Sens. 101, 89–101. http://dx.doi.org/10.1016/j.isprsjprs.2014.11.007.

Alexander, C., Moeslund, J.E., Bøcher, P.K., Arge, L., Svenning, J.-C., 2013. Airborne laser

scanner (LiDAR) proxies for understory light conditions. Remote Sens. Environ. 134, 152–161. http://dx.doi.org/10.1016/j.rse.2013.02.028.
Anderson, H.E., 1982. Aids to Determining Fuel Models for Estimating Fire Behavior (General Technical Report No. INT-122). USDA Forest Service, Intermountain Forest and Range Experiment Station, Ogden, UT.
Bartemucci, P., Messier, C., Canham, C.D., 2006. Overstory influences on light attenuation patterns and understory plant community diversity and composition in southern boreal forests of Quebec. Can. J. For. Res. 36, 2065–2079. http://dx.doi.org/10.1139/x06-088.
Ben-Arie, J.R., Hay, G.J., Powers, R.P., Castilla, G., St-Onge, B., 2009. Development of a pit filling algorithm for LiDAR canopy height models. Comput. Geosci. 35, 1940–1949. http://dx.doi.org/10.1016/j.cageo.2009.02.003.
Booth, D.T., Cox, S.E., Johnson, D.E., 2005. Detection-threshold calibration and other factors influencing digital measurements of ground cover. Rangel. Ecol. Manag. 58, 598–604. http://dx.doi.org/10.2111/05-060R1.1.
Boyd, C.S., Svejcar, T., 2005. A visual obstruction technique for photo monitoring of willow clumps. Rangel. Ecol. Manag. 58, 434–438. http://dx.doi.org/10.2111/1551-5028(2005)058[0434:AVOTFP]2.0.CO;2.
Brandtberg, T., 2007. Classifying individual tree species under leaf-off and leaf-on conditions using airborne lidar. ISPRS J. Photogramm. Remote Sens. 61, 325–340. http://dx.doi.org/10.1016/j.isprsjprs.2006.10.006.
Bright, B.C., Hudak, A.T., McGaughey, R., Andersen, H.-E., Negrón, J., 2013. Predicting live and dead tree basal area of bark beetle affected forests from discrete-return lidar. Can. J. Remote. Sens. 39, S99–S111. http://dx.doi.org/10.5589/m13-027.
Campbell, M.J., Dennison, P.E., Butler, B.W., 2017a. A LiDAR-based analysis of the effects of slope, vegetation density, and ground surface roughness on travel rates for wildland firefighter escape route mapping. Int. J. Wildland Fire 26, 884–895. http://dx.doi.org/10.1071/WF17031.
Campbell, M.J., Dennison, P.E., Butler, B.W., 2017b. Safe separation distance score: a new metric for evaluating wildland firefighter safety zones using lidar. Int. J. Geogr. Inf. Sci. 31, 1448–1466. http://dx.doi.org/10.1080/13658816.2016.1270453.
Carlyle, C.N., Fraser, L.H., Haddow, C.M., Bings, B.A., Harrower, W., 2010. The use of digital photos to assess visual cover for wildlife in rangelands. J. Environ. Manag. 91, 1366–1370. http://dx.doi.org/10.1016/j.jenvman.2010.02.018.
Chasmer, L., Hopkinson, C., Treitz, P., 2006. Investigating laser pulse penetration through a conifer canopy by integrating airborne and terrestrial lidar. Can. J. Remote. Sens. 32, 116–125. http://dx.doi.org/10.5589/m06-011.
Chen, Q., Gong, P., Baldocchi, D., Tian, Y.Q., 2007. Estimating basal area and stem volume for individual trees from lidar data. Photogramm. Eng. Remote. Sens. 73, 1355–1365. http://dx.doi.org/10.14358/PERS.73.12.1355.
Clark, M.L., Clark, D.B., Roberts, D.A., 2004. Small-footprint lidar estimation of sub-canopy elevation and tree height in a tropical rain forest landscape. Remote Sens. Environ. 91, 68–89. http://dx.doi.org/10.1016/j.rse.2004.02.008.
Clark, M.L., Roberts, D.A., Ewel, J.J., Clark, D.B., 2011. Estimation of tropical rain forest aboveground biomass with small-footprint lidar and hyperspectral sensors. Remote Sens. Environ. 115, 2931–2942. http://dx.doi.org/10.1016/j.rse.2010.08.029.
Collins, W.B., Becker, E.F., 2001. Estimation of horizontal cover. J. Range Manag. 54, 67–70. http://dx.doi.org/10.2307/4003530.
Dalponte, M., Bruzzone, L., Gianelle, D., 2011. A system for the estimation of single-tree stem diameter and volume using multireturn LIDAR data. IEEE Trans. Geosci. Remote Sens. 49, 2479–2490. http://dx.doi.org/10.1109/TGRS.2011.2107744.
Drake, J.B., Dubayah, R.O., Clark, D.B., Knox, R.G., Blair, J.B., Hofton, M.A., Chazdon, R.L., Weishampel, J.F., Prince, S., 2002. Estimation of tropical forest structural characteristics using large-footprint lidar. Remote Sens. Environ. 79, 305–319. http://dx.doi.org/10.1016/S0034-4257(01)00281-4.
Duebbert, H.F., Lokemoen, J.T., 1976. Duck nesting in fields of undisturbed grass-legume cover. J. Wildl. Manag. 40, 39–49. http://dx.doi.org/10.2307/3800154.
Eskelson, B.N.I., Madsen, L., Hagar, J.C., Temesgen, H., 2011. Estimating riparian understory vegetation cover with beta regression and copula models. For. Sci. 57, 212–221.
Estornell, J., Ruiz, L.A., Velázquez-Martí, B., Fernández-Sarría, A., 2011. Estimation of shrub biomass by airborne LiDAR data in small forest stands. For. Ecol. Manag. 262, 1697–1703. http://dx.doi.org/10.1016/j.foreco.2011.07.026.
Evans, J.S., Hudak, A.T., Faux, R., Smith, A.M.S., 2009. Discrete return lidar in natural resources: recommendations for project planning, data processing, and deliverables. Remote Sens. 1, 776–794. http://dx.doi.org/10.3390/rs1040776.
Falkowski, M.J., Smith, A.M.S., Gessler, P.E., Hudak, A.T., Vierling, L.A., Evans, J.S., 2008. The influence of conifer forest canopy cover on the accuracy of two individual tree measurement algorithms using lidar data. Can. J. Remote. Sens. 34, S338–S350. http://dx.doi.org/10.5589/m08-055.
Falkowski, M.J., Hudak, A.T., Crookston, N.L., Gessler, P.E., Uebler, E.H., Smith, A.M.S., 2010. Landscape-scale parameterization of a tree-level forest growth model: a k-nearest neighbor imputation approach incorporating LiDAR data. Can. J. For. Res. 40, 184–199. http://dx.doi.org/10.1139/X09-183.
Goodwin, N.R., Coops, N.C., Bater, C., Gergel, S.E., 2007. Assessment of sub-canopy structure in a complex coniferous forest. In: Proceedings of the ISPR Workshop "Laser Scanning 2007 and SilviLaser 2007", Espoo, September 12–14, 2007, Finland, pp. 169–172.
Griffith, B., Youtie, B.A., 1988. Two devices for estimating foliage density and deer hiding cover. Wildl. Soc. Bull. 1973–2006 (16), 206–210.
Hamraz, H., Contreras, M.A., Zhang, J., 2017. Forest understory trees can be segmented accurately within sufficiently dense airborne laser scanning point clouds. Sci. Rep. 7 (6770). http://dx.doi.org/10.1038/s41598-017-07200-0.
Higgins, K.F., Jenkins, K.J., Clambey, G.K., Uresk, D.W., Naugle, D., Norland, J., Barker, W.T., 2005. Vegetation sampling and measurement. In: Techniques for Wildlife Investigations and Management. The Wildlife Society, Bethesda, MD, pp. 524–553.
Hijmans, R.J., van Etten, J., Cheng, J., Mattiuzzi, M., Sumner, M., Greenberg, J.A., Lamigueiro, O.P., Bevan, A., Racine, E.B., Shortridge, A., 2016. Raster: Geographic Data Analysis and Modeling.
Hill, R.A., Broughton, R.K., 2009. Mapping the understorey of deciduous woodland from leaf-on and leaf-off airborne LiDAR data: a case study in lowland Britain. ISPRS J. Photogramm. Remote Sens. 64, 223–233. http://dx.doi.org/10.1016/j.isprsjprs.2008.12.004.
Holmgren, J., Nilsson, M., Olsson, H., 2003. Simulating the effects of lidar scanning angle for estimation of mean tree height and canopy closure. Can. J. Remote. Sens. 29, 623–632. http://dx.doi.org/10.5589/m03-030.
Hopkinson, C., Chasmer, L., Lim, K., Treitz, P., Creed, I., 2006. Towards a universal lidar canopy height indicator. Can. J. Remote. Sens. 32, 139–152. http://dx.doi.org/10.5589/m06-006.
Hudak, A.T., Crookston, N.L., Evans, J.S., Falkowski, M.J., Smith, A.M., Gessler, P.E., Morgan, P., 2006. Regression modeling and mapping of coniferous forest basal area and tree density from discrete-return lidar and multispectral satellite data. Can. J. Remote. Sens. 32, 126–138. http://dx.doi.org/10.5589/m06-007.
Hudak, A.T., Crookston, N.L., Evans, J.S., Hall, D.E., Falkowski, M.J., 2008. Nearest neighbor imputation of species-level, plot-scale forest structure attributes from LiDAR data. Remote Sens. Environ. 112, 2232–2245. http://dx.doi.org/10.1016/j.rse.2007.10.009.
Isenburg, M., 2015. LAStools. rapidlasso GmbH, Gilching, Germany.
Jakubowksi, M.K., Guo, Q., Collins, B., Stephens, S., Kelly, M., 2013. Predicting surface fuel models and fuel metrics using lidar and CIR imagery in a dense mixed conifer forest. Photogramm. Eng. Remote. Sens. 79, 37–49.
Jones, R.E., 1968. A board to measure cover used by prairie grouse. J. Wildl. Manag. 32, 28–31. http://dx.doi.org/10.2307/3798233.
Jorgensen, C.F., Stutzman, R.J., Anderson, L.C., Decker, S., E., Powell, L.A., Schacht, W.H., Fontaine, J.J., 2013. Choosing a DIVA: a comparison of emerging digital imagery vegetation analysis techniques. Appl. Veg. Sci. 16, 552–560. http://dx.doi.org/10.1111/avsc.12037.
Keane, R.E., 2014. Wildland Fuel Fundamentals and Applications. Springer.
Kerns, B.K., Ohmann, J.L., 2004. Evaluation and prediction of shrub cover in coastal Oregon forests (USA). Ecol. Indic. 4, 83–98. http://dx.doi.org/10.1016/j.ecolind.2003.12.002.
Khosravipour, A., Skidmore, A.K., Wang, T., Isenburg, M., Khoshelham, K., 2015. Effect of slope on treetop detection using a LiDAR Canopy Height Model. ISPRS J. Photogramm. Remote Sens. 104, 44–52. http://dx.doi.org/10.1016/j.isprsjprs.2015.02.013.
Korhonen, L., Korpela, I., Heiskanen, J., Maltamo, M., 2011. Airborne discrete-return LIDAR data in the estimation of vertical canopy cover, angular canopy closure and leaf area index. Remote Sens. Environ. 115, 1065–1080. http://dx.doi.org/10.1016/j.rse.2010.12.011.
Korpela, I., Ørka, H., Maltamo, M., Tokola, T., Hyyppä, J., Tokola, M., Maltamo, T., 2010. Tree species classification using airborne LiDAR - effects of stand and tree parameters, downsizing of training set, intensity normalization, and sensor type. Silva Fennica 44, 319–339. http://dx.doi.org/10.14214/sf.156.
Korpela, I., Hovi, A., Morsdorf, F., 2012. Understory trees in airborne LiDAR data — selective mapping due to transmission losses and echo-triggering mechanisms. Remote Sens. Environ. 119, 92–104. http://dx.doi.org/10.1016/j.rse.2011.12.011.
Kramer, H.A., Collins, B.M., Lake, F.K., Jakubowski, M.K., Stephens, S.L., Kelly, M., 2016. Estimating ladder fuels: a new approach combining field photography with LiDAR. Remote Sens. 8, 766. http://dx.doi.org/10.3390/rs8090766.
Kükenbrink, D., Schneider, F.D., Leiterer, R., Schaepman, M.E., Morsdorf, F., 2017. Quantification of hidden canopy volume of airborne laser scanning data using a voxel traversal algorithm. Remote Sens. Environ. 194, 424–436. http://dx.doi.org/10.1016/j.rse.2016.10.023.
Latifi, H., Nothdurft, A., Koch, B., 2010. Non-parametric prediction and mapping of standing timber volume and biomass in a temperate forest: application of multiple optical/LiDAR-derived predictors. Forestry 83, 395–407. http://dx.doi.org/10.1093/forestry/cpq022.
Lefsky, M.A., Harding, D., Cohen, W.B., Parker, G., Shugart, H.H., 1999. Surface lidar remote sensing of basal area and biomass in deciduous forests of Eastern Maryland, USA. Remote Sens. Environ. 67, 83–98. http://dx.doi.org/10.1016/S0034-4257(98)00071-6.
Limb, R.F., Hickman, K.R., Engle, D.M., Norland, J.E., Fuhlendorf, S.D., 2007. Digital photography: reduced investigator variation in visual obstruction measurements for southern tallgrass prairie. Rangel. Ecol. Manag. 60, 548–552. http://dx.doi.org/10.2111/1551-5028(2007)60[548:DPRIVI]2.0.CO;2.
Lone, K., Loe, L.E., Gobakken, T., Linnell, J.D.C., Odden, J., Remmen, J., Mysterud, A., 2014. Living and dying in a multi-predator landscape of fear: roe deer are squeezed by contrasting pattern of predation risk imposed by lynx and humans. Oikos 123, 641–651. http://dx.doi.org/10.1111/j.1600-0706.2013.00938.x.
Maltamo, M., Mustonen, K., Hyyppä, J., Pitkänen, J., Yu, X., 2004. The accuracy of estimating individual tree variables with airborne laser scanning in a boreal nature reserve. Can. J. For. Res. 34, 1791–1801. http://dx.doi.org/10.1139/x04-055.
Maltamo, M., Packalén, P., Yu, X., Eerikäinen, K., Hyyppä, J., Pitkänen, J., 2005. Identifying and quantifying structural characteristics of heterogeneous boreal forests using laser scanner data. For. Ecol. Manag. 216, 41–50. http://dx.doi.org/10.1016/j.foreco.2005.05.034.
Marsden, S.J., Fielding, A.H., Mead, C., Hussin, M.Z., 2002. A technique for measuring the density and complexity of understorey vegetation in tropical forests. For. Ecol. Manag. 165, 117–123. http://dx.doi.org/10.1016/S0378-1127(01)00653-3.
Martinuzzi, S., Vierling, L.A., Gould, W.A., Falkowski, M.J., Evans, J.S., Hudak, A.T., Vierling, K.T., 2009. Mapping snags and understory shrubs for a LiDAR-based assessment of wildlife habitat suitability. Remote Sens. Environ. 113, 2533–2546.

Meng, X., Currit, N., Zhao, K., 2010. Ground filtering algorithms for airborne LiDAR Data: a review of critical issues. Remote Sens. 2, 833–860. http://dx.doi.org/10.3390/rs2030833.
Minasny, B., McBratney, A.B., 2006. A conditioned Latin hypercube method for sampling in the presence of ancillary information. Comput. Geosci. 32, 1378–1388. http://dx.doi.org/10.1016/j.cageo.2005.12.009.
Morrison, L.W., 2016. Observer error in vegetation surveys: a review. J. Plant Ecol. 9, 367–379. http://dx.doi.org/10.1093/jpe/rtv077.
Morsdorf, F., Mårell, A., Koetz, B., Cassagne, N., Pimont, F., Rigolot, E., Allgöwer, B., 2010. Discrimination of vegetation strata in a multi-layered Mediterranean forest ecosystem using height and intensity information derived from airborne laser scanning. Remote Sens. Environ. 114, 1403–1415. http://dx.doi.org/10.1016/j.rse.2010.01.023.
Musil, D.D., Reese, K.P., Connelly, J.W., 1994. Nesting and summer habitat use by translocated sage grouse (Centrocercus urophasianus) in Central Idaho. The Great Basin Naturalist 54, 228–233.
Mutlu, M., Popescu, S.C., Stripling, C., Spencer, T., 2008. Mapping surface fuel models using lidar and multispectral data fusion for fire behavior. Remote Sens. Environ. 112, 274–285. http://dx.doi.org/10.1016/j.rse.2007.05.005.
Næsset, E., 2002. Predicting forest stand characteristics with airborne scanning laser using a practical two-stage procedure and field data. Remote Sens. Environ. 80, 88–99. http://dx.doi.org/10.1016/S0034-4257(01)00290-5.
Nijland, W., Nielsen, S.E., Coops, N.C., Wulder, M.A., Stenhouse, G.B., 2014. Fine-spatial scale predictions of understory species using climate- and LiDAR-derived terrain and canopy metrics. JARS, JARSC4 8 (083572). http://dx.doi.org/10.1117/1.JRS.8.083572.
Nudds, T.D., 1977. Quantifying the vegetative structure of wildlife cover. Wildl. Soc. Bull. 1973–2006 (5), 113–117.
Penner, M., Pitt, D.G., Woods, M.E., 2013. Parametric vs. nonparametric LiDAR models for operational forest inventory in boreal Ontario. Can. J. Remote. Sens. 39, 426–443. http://dx.doi.org/10.5589/m13-049.
Pesonen, A., Maltamo, M., Eerikäinen, K., Packalèn, P., 2008. Airborne laser scanning-based prediction of coarse woody debris volumes in a conservation area. For. Ecol. Manag. 255, 3288–3296. http://dx.doi.org/10.1016/j.foreco.2008.02.017.
Popescu, S.C., Wynne, R.H., Nelson, R.F., 2002. Estimating plot-level tree heights with lidar: local filtering with a canopy-height based variable window size. Comput. Electron. Agric. 37, 71–95. http://dx.doi.org/10.1016/S0168-1699(02)00121-7.
R Core Team, 2016. R: A Language and Environment for Statistical Computing. R Foundation for Statistical Computing, Vienna, Austria.
Reutebuch, S.E., McGaughey, R.J., Andersen, H.-E., Carson, W.W., 2003. Accuracy of a high-resolution lidar terrain model under a conifer forest canopy. Can. J. Remote. Sens. 29, 527–535. http://dx.doi.org/10.5589/m03-022.
Riaño, D., Meier, E., Allgower, B., Chuvieco, E., Ustin, S.L., 2003. Modeling airborne laser scanning data for the spatial generation of critical forest parameters in fire behavior modeling. Remote Sens. Environ. 86, 177–186. http://dx.doi.org/10.1016/S0034-4257(03)00098-1.
Riaño, D., Valladares, F., Condés, S., Chuvieco, E., 2004. Estimation of leaf area index and covered ground from airborne laser scanner (Lidar) in two contrasting forests. Agric. For. Meteorol. 124, 269–275. http://dx.doi.org/10.1016/j.agrformet.2004.02.005.
Richardson, J.J., Moskal, L.M., 2011. Strengths and limitations of assessing forest density and spatial configuration with aerial LiDAR. Remote Sens. Environ. 115, 2640–2651. http://dx.doi.org/10.1016/j.rse.2011.05.020.
Richardson, J.J., Moskal, L.M., Kim, S.-H., 2009. Modeling approaches to estimate effective leaf area index from aerial discrete-return LIDAR. Agric. For. Meteorol. 149, 1152–1160. http://dx.doi.org/10.1016/j.agrformet.2009.02.007.
Robel, R.J., Briggs, J.N., Dayton, A.D., Hulbert, L.C., 1970. Relationships between visual obstruction measurements and weight of grassland vegetation. J. Range Manag. 23, 295–297. http://dx.doi.org/10.2307/3896225.
Roudier, P., 2017. clhs: Conditioned Latin Hypercube Sampling.
Sage, R., Hollins, K., Gregory, C., L., Woodburn, M., Carroll, J., 2004. Impact of roe deer Capreolus capreolus browsing on understorey vegetation in small farm woodlands. Wildl. Biol. 10, 115–120.
Seielstad, C.A., Queen, L.P., 2003. Using airborne laser altimetry to determine fuel models for estimating fire behavior. J. For. 101, 10–15.
Singh, K.K., Davis, A.J., Meentemeyer, R.K., 2015. Detecting understory plant invasion in urban forests using LiDAR. Int. J. Appl. Earth Obs. Geoinf. 38, 267–279. http://dx.doi.org/10.1016/j.jag.2015.01.012.
Skowronski, N., Clark, K., Nelson, R., Hom, J., Patterson, M., 2007. Remotely sensed measurements of forest structure and fuel loads in the pinelands of New Jersey. Remote Sensing of Environment, The Application of Remote Sensing to Fire Research in the Eastern United States 108, 123–129. http://dx.doi.org/10.1016/j.rse.2006.09.032.
Smith, A.M.S., Falkowski, M.J., Hudak, A.T., Evans, J.S., Robinson, A.P., Steele, C.M., 2009. A cross-comparison of field, spectral, and lidar estimates of forest canopy cover. Can. J. Remote. Sens. 35, 447–459. http://dx.doi.org/10.5589/m09-038.
Stephens, S.L., 1998. Evaluation of the effects of silvicultural and fuels treatments on potential fire behaviour in Sierra Nevada mixed-conifer forests. For. Ecol. Manag. 105, 21–35. http://dx.doi.org/10.1016/S0378-1127(97)00293-4.
Su, J.G., Bork, E.W., 2006. Influence of vegetation, slope, and lidar sampling angle on DEM accuracy. Photogramm. Eng. Remote. Sens. 72, 1265–1274. http://dx.doi.org/10.14358/PERS.72.11.1265.
Su, J.G., Bork, E.W., 2007. Characterization of diverse plant communities in aspen parkland rangeland using LiDAR data. Appl. Veg. Sci. 10, 407–416. http://dx.doi.org/10.1658/1402-2001(2007)10[407:CODPCI]2.0.CO;2.
Suchar, V.A., Crookston, N.L., 2010. Understory cover and biomass indices predictions for forest ecosystems of the r United States. Ecol. Indic. 10, 602–609. http://dx.doi.org/10.1016/j.ecolind.2009.10.004.
Takahashi, T., Yamamoto, K., Miyachi, Y., Senda, Y., Tsuzuku, M., 2006. The penetration rate of laser pulses transmitted from a small-footprint airborne LiDAR: a case study in closed canopy, middle-aged pure sugi (Cryptomeria japonica D. Don) and hinoki cypress (Chamaecyparis obtusa Sieb. et Zucc.) stands in Japan. J. For. Res. 11, 117–123. http://dx.doi.org/10.1007/s10310-005-0189-0.
Tang, H., Brolly, M., Zhao, F., Strahler, A.H., Schaaf, C.L., Ganguly, S., Zhang, G., Dubayah, R., 2014. Deriving and validating Leaf Area Index (LAI) at multiple spatial scales through lidar remote sensing: a case study in Sierra National Forest, CA. Remote Sens. Environ. 143, 131–141. http://dx.doi.org/10.1016/j.rse.2013.12.007.
USDA Forest Service, 2014. First order lidar metrics: A supporting document for lidar deliverables [WWW Document]. URL. https://www.fs.fed.us/eng/rsac/lidar_training/pdf/LidarMetricsDescriptionOfDeliverables_Generic_12_15_14.pdf (accessed 10.7.17).
USDA Forest Service, 2017. Monroe Mountain Aspen Ecosystems Restoration Project [WWW Document]. URL. https://usfs.maps.arcgis.com/apps/MapJournal/index.html?appid=6c17eb611f7a4578b5e28681ca684432 accessed 10.11.17.
Vaglio Laurin, G., Puletti, N., Chen, Q., Corona, P., Papale, D., Valentini, R., 2016. Above ground biomass and tree species richness estimation with airborne lidar in tropical Ghana forests. Int. J. Appl. Earth Obs. Geoinf. 52, 371–379. http://dx.doi.org/10.1016/j.jag.2016.07.008.
Wing, B.M., Ritchie, M.W., Boston, K., Cohen, W.B., Gitelman, A., Olsen, M.J., 2012. Prediction of understory vegetation cover with airborne lidar in an interior ponderosa pine forest. Remote Sens. Environ. 124, 730–741. http://dx.doi.org/10.1016/j.rse.2012.06.024.
Winnard, A.L., Di Stefano, J., Coulson, G., 2013. Habitat use of a critically-endangered species in a predator-free but degraded reserve in Australia. Wildl. Biol. 19, 429–438. http://dx.doi.org/10.2981/12-116.
Wulder, M.A., Coops, N.C., Hudak, A.T., Morsdorf, F., Nelson, R., Newnham, G., Vastaranta, M., 2013. Status and prospects for LiDAR remote sensing of forested ecosystems. Can. J. Remote. Sens. 39, S1–S5. http://dx.doi.org/10.5589/m13-051.
Zhang, X., Friedl, M.A., Schaaf, C.B., Strahler, A.H., Hodges, J.C.F., Gao, F., Reed, B.C., Huete, A., 2003. Monitoring vegetation phenology using MODIS. Remote Sens. Environ. 84, 471–475. http://dx.doi.org/10.1016/S0034-4257(02)00135-9.